Evaluation of Several A-Train Ice Cloud Retrieval Products with In Situ Measurements Collected during the SPARTICUS Campaign

MIN DENG

University of Wyoming, Laramie, Wyoming

GERALD G. MACE

University of Utah, Salt Lake City, Utah

ZHIEN WANG

University of Wyoming, Laramie, Wyoming

R. PAUL LAWSON

Stratton Park Engineering Company, Inc., Boulder, Colorado

ABSTRACT

In this study several ice cloud retrieval products that utilize active and passive A-Train measurements are evaluated using in situ data collected during the Small Particles in Cirrus (SPARTICUS) field campaign. The retrieval datasets include ice water content (IWC), effective radius r_e, and visible extinction σ from *CloudSat* level-2C ice cloud property product (2C-ICE), *CloudSat* level-2B radar-visible optical depth cloud water content product (2B-CWC-RVOD), radar–lidar (DARDAR), and σ from *Cloud–Aerosol Lidar and Infrared Pathfinder Satellite Observations* (*CALIPSO*). When the discrepancies between the radar reflectivity Z_e derived from 2D stereo probe (2D-S) in situ measurements and Z_e measured by the *CloudSat* radar are less than 10 dBZ_e, the flight mean ratios of the retrieved IWC to the IWC estimated from in situ data are 1.12, 1.59, and 1.02, respectively for 2C-ICE, DARDAR, and 2B-CWC-RVOD. For r_e, the flight mean ratios are 1.05, 1.18, and 1.61, respectively. For σ, the flight mean ratios for 2C-ICE, DARDAR, and *CALIPSO* are 1.03, 1.42, and 0.97, respectively. The *CloudSat* 2C-ICE and DARDAR retrieval products are typically in close agreement. However, the use of parameterized radar signals in ice cloud volumes that are below the detection threshold of the *CloudSat* radar in the 2C-ICE algorithm provides an extra constraint that leads to slightly better agreement with in situ data. The differences in assumed mass–size and area–size relations between *CloudSat* 2C-ICE and DARDAR also contribute to some subtle difference between the datasets: r_e from the 2B-CWC-RVOD dataset is biased more than the other retrieval products and in situ measurements by about 40%. A slight low (negative) bias in *CALIPSO* σ may be due to 5-km averaging in situations in which the cirrus layers have significant horizontal gradients in σ.

1. Introduction

CloudSat is one of the five satellites in the A-Train constellation. A vertical profile of radar reflectivity factor Z_e is measured by the 94-GHz cloud profiling radar (CPR; Im et al. 2006) at a vertical resolution of 240 m between the surface and 30-km altitude. The footprint size is approximately 1.3 km across track by 1.7 km along track. The CPR has a minimum sensitivity of ~ -30 dBZ_e (Stephens et al. 2008). During the period of this study, *Cloud–Aerosol Lidar and Infrared Pathfinder Satellite Observations* (*CALIPSO*) followed *CloudSat* by no more than 15 s. The *CALIPSO* lidar (Winker et al. 2009) measures parallel and perpendicular attenuated backscatter β at 532 nm and total backscatter at 1064 nm at vertical and along-track resolutions that are altitude dependent (60-m vertical resolution with footprints

Corresponding author address: Min Deng, Department of Atmospheric Science, University of Wyoming, Dept. 3038, 1000 E. University Ave., Laramie, WY 82071.
E-mail: mdeng2@uwyo.edu

averaged to ~1.0 km along track between 8.2 and 20.2 km and 30-m vertical and 0.333-km along-track resolution below 8.2 km). The datasets produced by these two active remote sensors, when combined with the passive remote sensors of the A-Train constellation (Stephens et al. 2008), have provided an unprecedented global view of clouds (Sassen et al. 2009; G. G. Mace et al. 2009) and precipitation (Stephens et al. 2010) and also motivated development of a series of cloud property retrieval algorithms using various combinations of radar, lidar, and radiometer measurements (Austin and Stephens 2001; Hogan et al. 2006; Young and Vaughan 2009; Delanoë and Hogan 2008, 2010; Deng et al. 2010; Mace 2010).

Because ice clouds are composed of nonspherical ice crystals with bulk microphysical properties that cover a wide dynamic range that depend on their formation mechanism, history, and dynamic and thermodynamics atmospheric states, many assumptions are often necessary to reduce the inversion of the remote sensing data to a tractable problem. Therefore, uncertainties in ice cloud property retrievals can be substantial. While algorithm developers often work to reduce biases, it is difficult to determine quantitatively how accurate the algorithms are under specific circumstances. While data collected in situ have their own set of problems, these problems are often different and also often more manageable than those confronting remote sensing inversion algorithms. Therefore, in situ data can be quite useful in identifying shortcomings in remote sensing retrievals that arise because of assumptions in the inversion process. In this paper, we evaluate several ice cloud retrieval products with data collected during a long-term in situ measurement campaign called Small Particles in Cirrus (SPARTICUS, from January to June 2010; J. Mace et al. 2009) funded by the U.S. Department of Energy Atmospheric Radiation Measurement Program (DOE ARM; Ackerman and Stokes 2003).

This paper is organized as follows. First, the retrieval datasets and in situ measurements are introduced in section 2 followed by the evaluation methodology in section 3. Then we examine several case studies to evaluate algorithm performance in different radar and lidar measurement situations in section 4 where the retrieval results are discussed within the context provided by the in situ measurements. In section 5, statistical comparisons are presented that show the relationships among the algorithms. The relationships among the ice water content (IWC), extinction coefficients r_e, and radar reflectivity are investigated in comparison with the in situ measurement dataset. In the last section, we present our conclusions and summary.

2. Satellite retrieval products and the SPARTICUS project

a. 2C-ICE

The *CloudSat* and *CALIPSO* level-2C ice cloud property product (2C-ICE; Deng et al. 2010) is a standard operational *CloudSat* dataset that is publicly available through the *CloudSat* data processing center at Colorado State University. The 2C-ICE data provide a vertically resolved retrieval of ice cloud properties such as r_e, IWC, and visible extinction σ by synergistically combining *CloudSat* Z_e and *CALIPSO* β at 532 nm at the *CloudSat* horizontal and vertical resolutions based on an optimal estimation framework. Lidar multiple scattering is accounted for using a constant factor for a fast lidar forward model calculation. Lidar ratio (extinction to backscattering ratio) is assumed to be constant in the 2C-ICE version that is evaluated in this paper. The forward model assumes a first-order gamma particle size distribution (PSD) of idealized nonspherical ice crystals (Yang et al. 2000). The Mie scattering of radar reflectivity is calculated in the forward model lookup table according a discrete dipole approximation (DDA) by Hong (2007).

The characteristics of the instruments convolved on the physical properties of clouds in the upper troposphere require us to consider that three distinct radar–lidar regions could exist in any ice cloud layer. For the lidar-only region, where Z_e is below the CPR detection threshold, the radar signal is parameterized using DOE ARM ground-based Millimeter Cloud Radar (MMCR) observations so that the retrieval can still be loosely constrained with two inputs. When the lidar signal is unavailable because of strong attenuation (i.e., the radar-only region), the retrieval tends toward an empirical relationship using the radar reflectivity factor and temperature (Hogan et al. 2006; Liu and Illingworth 2000). Readers desiring a more in-depth description of the 2C-ICE algorithm should refer to Deng et al. (2010) for details. The algorithm has been applied to *CloudSat/ CALIPSO* data as well as lidar and radar data collected by the ER-2 during the Tropical Composition, Cloud, and Climate Coupling (TC4) mission (Toon et al. 2010). The retrieved r_e, IWC, and σ are shown to compare favorably to coincident in situ measurements collected by instruments on the National Aeronautics and Space Administration (NASA) DC-8. For example, we calculated the mean and median and standard deviation of the counterflow virtual impactor (CVI)/2C-ICE and 2D stereo probe (2D-S)/2C-ICE IWC ratios for the cases in Deng et al. (2010). For the ER-2 case (Figs. 9 and 10 of Deng et al. 2010), the median, mean, and standard deviation of the CVI/2C-ICE and 2D-S/2C-ICE IWCs

were 1.05, 1.21, and ±2.51 and 0.69, 0.78, and ±0.46, respectively. For the *CloudSat* and *CALIPSO* case (Figs. 11 and 12 of Deng et al. 2010), the median, mean, and standard deviation of the CVI/2C-ICE and 2D-S/2C-ICE IWCs were 1.31, 1.74, and ±3.2 and 1.09, 1.54, and ±4.1, respectively. Based on the IWCs from two instruments, we conclude that the uncertainty of 2C-ICE IWC is around 30%.

b. DARDAR

Similar to the 2C-ICE product, the radar–lidar (DARDAR) cloud product is a synergetic ice cloud retrieval algorithm derived from the combination of the *CloudSat* Z_e and *CALIPSO* β using a variational method for retrieving profiles of σ, IWC, and r_e. DARDAR was developed at the University of Reading by J. Delanoë and R. Hogan (Delanoë and Hogan 2008, 2010). There are several differences between 2C-ICE and DARDAR. First, DARDAR is retrieved using the *CALIPSO* vertical resolution (60 m) instead of the *CloudSat* vertical resolution as in 2C-ICE. Second, the multiple scattering in the lidar signal is accounted with a fast multiple-scattering code (Hogan 2006) instead of assuming a constant multiple-scattering factor as in 2C-ICE. Third, the lidar backscatter to extinction ratio is retrieved rather than assumed to be a constant as in 2C-ICE. Fourth, no parameterizations of radar or lidar signals are used for the lidar-only or radar-only regions of the ice cloud profile. Empirical relationships are heavily relied on for those regions in the DARDAR algorithm. Fifth, the DARDAR product assumes a "unified" PSD given by Field et al. (2005). The mass–size and area–size relation of nonspherical particles is considered using relationships derived from in situ measurements (Francis et al. 1998; Brown and Francis 1995).

c. CWC-RVOD

The *CloudSat* level-2B radar-visible optical depth cloud water content product (2B-CWC-RVOD) contains estimates of cloud liquid and ice water content and effective radius that is derived using a combination of Z_e together with estimates of visible optical depth derived from Moderate Resolution Imaging Spectroradiometer (MODIS) reflectances [from the *CloudSat* level-2B cloud optical depth product (2B-TAU)] to constrain the cloud retrievals more tightly than in the level-2B radar-only cloud water content product (2B-CWC-RO; Austin et al. 2009) presumably yielding more accurate results.

The forward model in the retrieval algorithm assumes the ice particles to be spheres with a lognormal PSD. IWC is defined as the third moment of the PSD over all possible ice particle sizes assuming a constant ice density

($\rho_i = 917$ kg m^{-3}). The optimization iteration is initialized with an a priori PSD specified by the temperature dependences obtained from in situ data (Austin et al. 2009), with the temperature information obtained from European Centre for Medium-Range Weather Forecasts operational analyses. Several ice cloud microphysical retrieval algorithms are compared in Heymsfield et al. (2008), using simulated reflectivity and optical depth values based on cloud probe measurements. The mean retrieved-to-measured ratio for IWC from the *CloudSat* 2B-CWC-RVOD algorithm is found to be 1.27 ± 0.78 when equivalent radar reflectivity is greater than -28 dBZ_e. While most of the IWC retrievals are within ±25% of the true value, the algorithm exhibits high bias of over 50% when IWC is less than ~100 mg m^{-3}, with some of the biases related to the potential errors in the measured extinction for small ice crystals in the probe data; therefore the estimated systematic error for IWC is likely ±40% (Heymsfield et al. 2008).

d. CALIPSO extinction at 5 km

The *CALIPSO* σ retrievals are provided at horizontal resolutions of 5, 20, and 80 km, which corresponds, respectively to averages of 15, 60, and 240 consecutive lidar profiles (Young and Vaughan 2009). In this study we use the 5-km data. In the retrieval, the lidar multiple scattering is considered a constant (0.6) as in the 2C-ICE product. There are two types of data labeled by data quality control information in the data files: constrained or unconstrained. Whenever possible, σ solutions are constrained by a determination of the two-way transmittance provided by the boundary location algorithm. To accomplish this, an adjustment of the particulate lidar ratio is made iteratively using a variable secant algorithm as described in Froberg (1965, section 2.2) until the retrieved particulate two-way transmittance differs from an assumed constraint by less than a specified tolerance. The assumption of constant lidar ratio in the *CALIPSO* retrieval is probably one of the largest factors affecting the lidar extinction comparisons. We found that the histogram of retrieved lidar ratio for constrained cases in 2007 peaked at 30 with a half-width of about 10 (not shown).

For the unconstrained cases, where the lidar signal is fully attenuated or in contact with the surface, the retrieval of correct extinction profiles obviously depends on the predetermined lidar ratio. However, for the algorithm iteration, the retrieved profile may diverge from the correct values if incorrect estimates of the lidar ratio, multiple-scattering function, or correction for the attenuation of overlying features are used. The *CALIPSO* team chooses to adjust the lidar ratio to prevent divergence in

features (Young and Vaughan 2009). Upon detecting divergence, the profile solver algorithm is terminated and then restarted using a modified value of the lidar ratio. For solutions diverging in the positive direction, the lidar ratio is reduced, and for solutions diverging in the negative direction, the lidar ratio is increased. These cases account for only about 3% of all ice cloud profiles based on data collected in 2007.

e. SPARTICUS

Comparison of different retrieval datasets provides information on algorithm consistency and reliability. Since there is no standard measurement of in situ microphysical cloud properties as the absolute truth for retrieval algorithm evaluation, it is presumptuous to call a comparison of remote retrievals with in situ measurements a "validation" of the retrieval products. Also, since there is no standard measurement for comparison, it is not possible to rigorously formulate an uncertainty (see, e.g., Abernethy and Benedict 1984; Bevington and Robinson 1992). However, with proper understanding of the limitations of both remote and in situ instrumentation, it is possible to compare the measurements, assess consistency, and formulate interpretations based on physical principals. Uncertainties in cloud particle probe measurements have been discussed by many investigators. For example, Korolev et al. (1998) and Korolev and Isaac (2005) discuss uncertainties in 2D cloud (2D-C) particle imaging probes. Lawson et al. (2006) discuss uncertainties in the 2D-S particle imaging probe. Korolev et al. (2011) discuss the effects of shattering on the 2D-C probes and cloud-imaging probes and Lawson (2011) discusses shattering on the 2D-S probe. The SPARTICUS field campaign, as a major effort of the DOE ARM Aerial Facility program, took place over the central United States from January through June 2010 using the Stratton Park Engineering Company, Inc. (SPEC), Lear 25 research aircraft (Lawson 2011). Approximately 200 h of research time were devoted to measurements in ice clouds over the ARM Southern Great Plains ground site as well as under the A-Train satellite constellation. SPARTICUS provides a collection of microphysical data that includes the 2D-S, measuring ice particle size distribution $10 < D < 3000$ μm. The 2D-S is a critical instrument for quantifying concentration of ice cloud particles because the probe and subsequent data analysis methodologies are designed to minimize the extent to which shattered ice crystal remnants bias reported particle numbers (Lawson et al. 2006; Lawson 2011). Processing of 2D-S image data is a complex process that has evolved based on both theoretical and empirical approaches. The processing can loosely be divided into three broad steps:

1) various methods to determine "characteristic" lengths and areas of an image,
2) removal of what are called here "spurious" events (also referred to as artifact rejection), which can include electronic noise, optical contamination, particle shattering and splashing effects, and
3) various methods Mi of estimating the bulk physical parameters; concentration, extinction, and mass as functions of size [these include correction for diffraction effects based on the Korolev (2007) method and adjustments to sample volume as a function of particle size].

For M1 processing we use the dimension along the direction of flight and include all particles, whether they are completely contained within the image frame (commonly referred to as "all in") or not. For M2, M4, and M6 processing we use the all-in technique. M4 processing also includes the Korolev (2007) correction for out of focus images. The SPARTICUS data were processed using M4 for sizes up to 365 μm, and MI for all larger images. See appendix A and B in Lawson (2011) for an explanation of the various "M" processing techniques and other details. Comparisons of 2D-S-derived IWC in aged tropical cirrus anvils agree very well with measurements from a counterflow virtual impactor (Twohy et al. 1997) in the TC4 field campaign (Mitchell et al. 2010; Lawson et al. 2010; Mace 2010). For example, for the ER-2 case evaluated in Deng et al. 2010, the median, mean, and standard deviation of the 2D-S/CVI IWC ratios are 0.66, 0.69, and ±0.31, respectively. For the *CloudSat* and *CALIPSO* case, the median, mean, and standard deviation of the 2D-S/CVI IWC ratios are 0.91, 1.33, and ±3.53, respectively.

The 2D-S estimates of cloud properties reported here are based on preliminary analysis and archiving by SPEC. The archived data are thought to be reliable; however, as with most datasets processed soon after a field campaign, refinements and improvements in data are an evolutionary process.

In cases with relatively high concentrations of millimeter-size particles, the 2D precipitation (2D-P) particle imaging probe (an external optical system that images particles in the size range 200–6400 μm) tends to overlap the 2D-S PSD and extend it to larger sizes. The SPEC version-3 High Volume Precipitation Spectrometer (HVPS) was installed for the last month (June 2010) of the SPARTICUS field campaign. Based on comparison between 2D-S and 2D-P or HVPS, no significant concentration of large particles (~1–3 mm) were observed by 2D-P or HVPS for the cases we are discussing in the paper, which indicates that 2D-S measurement alone is sufficient to estimate of the PSD moments assessed in this study.

During SPARTICUS, the SPEC Lear supported 21 overpasses of the NASA A-Train satellites to obtain cirrus size distribution data in conjunction with sampling by the orbiting remote sensing instruments. Figure 1 shows the retrieved IWC, r_e, and σ of 17 cases from DARDAR, 2B-CWC-RVOD, and *CALIPSO* σ in comparison with 2C-ICE retrievals. The DARDAR IWC, r_e, and σ in the radar region, which includes the radar–lidar overlap and radar-only regions are in reasonable agreement with 2C-ICE, while for the lidar-only region, the DARDAR IWC and σ coefficients are larger than 2C-ICE. The 2B-CWC-RVOD r_e is about 30% larger than r_e for 2C-ICE and DARDAR while IWC is slightly smaller. The *CALIPSO* σ is very scattered as compared with the DARDAR dataset. The overpass flights typically have long horizontal legs sampled during the overpass where the aircraft flew level within cirrus. In Table 1 we listed the 17 flight legs that are used in this study. In the following, the disparities among the retrieval products are investigated with in situ measurements.

3. Method

For the 17 cases evaluated here, estimates of r_e, IWC, and σ derived from A-Train data are compared to in situ estimates. In situ r_e are derived from the airborne estimates of IWC divided by image projected area. The image projected area measurements are also used to compute σ. Airborne estimates of IWC are estimated using projected area to mass relationships described in Baker and Lawson (2006). Although the mass is not a direct measurement, it has generally compared favorably to other mass in situ measurement such as CVI measurements during the TC4 project (Deng et al. 2010; Mace 2010; Mitchell et al. 2010; Lawson et al. 2010).

In Fig. 2, we show the minimum distance and time lag Δt between the SPEC Lear 25 and A-Train during 17 SPARTICUS flight legs. Case summaries are listed in Table 1. The distances between the Lear and the A-Train satellite tracks range from 1 to 5 km. The Δt between them are within 15 min except for cases 3 and 10. The flight mean temperatures ranged from 215 to 243 K.

Given the uncertainties in the in situ measurements and because of cloud spatial inhomogeneities and cloud field evolution with time, we seek to devise some criteria that will allow us to avoid obvious inconsistencies between the in situ and satellite data. Because Z_e is a basic measurable of *CloudSat* from which the microphysical properties of interest are derived, and because, at least for the cirrus clouds analyzed here, the 2D-S provides reasonable sampling in the particle size range that
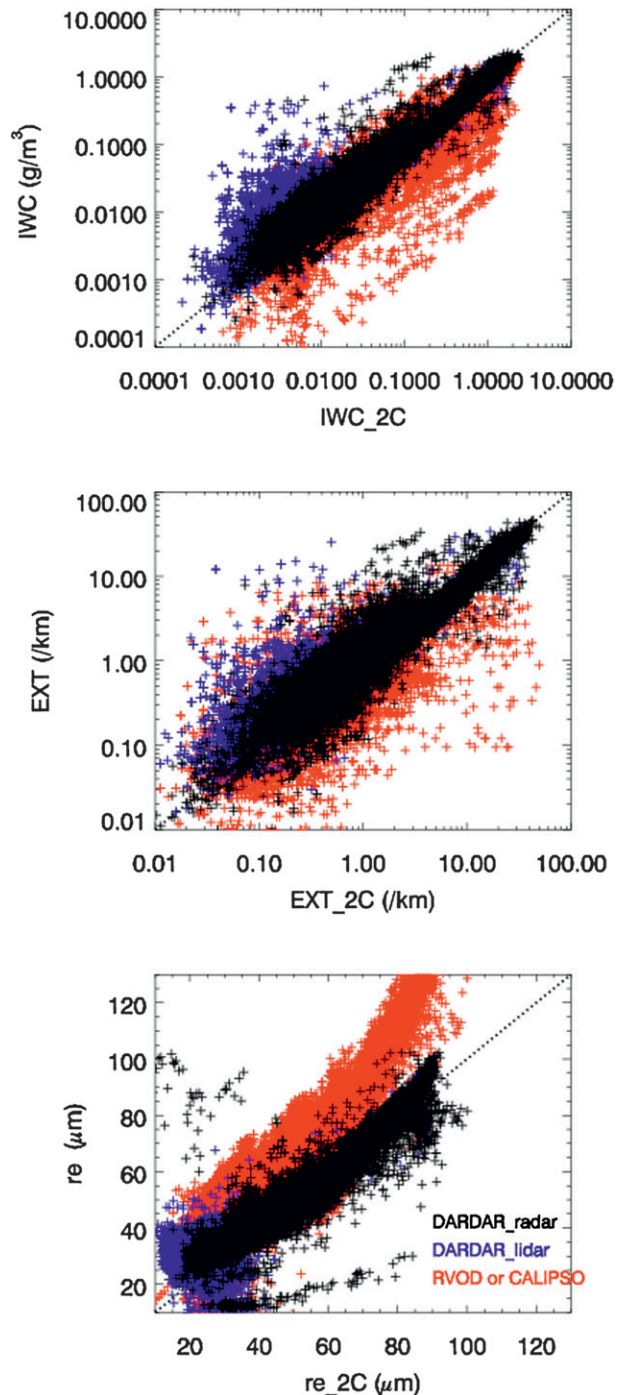

FIG. 1. Retrieved cloud properties from DARDAR, 2B-CWC-RVOD, and *CALIPSO* extinction in comparison with 2C-ICE for the 17 cases during the SPARTICUS project.

contributes to the cloud physical properties, discrepancies between in situ–estimated and *CloudSat*-measured Z_e offer a means of identifying periods when comparisons between the cloud volumes sampled by the Lear 25 and

TABLE 1. Summary of 17 flight legs of the SPEC Lear 25 underflying the A-Train. For r_e, IWC, and extinction coefficients, the four numbers are 2D-S leg mean and mean ratio of retrieved-to-measured for 2C-ICE, DARDAR, and 2B-CWC-RVOD (or *CALIPSO* extinction), respectively. For optical depth τ, the two numbers are leg mean optical depth and its std dev, respectively. Here r is the correlation coefficients of radar reflectivity between in situ–simulated and *CloudSat*-measured (or 2C-ICE-parameterized for the lidar-only region). The terms Δt and Δs are the time duration and minimum distance between the SPEC Lear 25 and NASA A-Train satellite, respectively. Italic cases are cases of thick clouds in which the SPEC Lear 25 mainly flew through the border of our defined radar-only and radar–lidar overlapped regions. Boldface cases are cases of very thin cloud in which the SPEC Lear 25 mainly flew through the lidar-only region.

Case	Date/leg	r_e (μm)	IWC (mg m^{-3})	Extinction (km^{-1})	τ	r	Δt (s)	Δs (km)	T (K)
1	**23 Jan**	**30.8/0.98/1.11/1.06**	**28.0/0.53/1.01/0.46**	**1.42/0.50/0.89/0.38**	**2.5 (1.8)**	**0.7**	**182**	**2.4**	**231**
2	**3 Feb**	**42.8/0.83/0.99/1.04**	**12.5/0.76/0.76/0.66**	**0.46/0.82/0.79/0.45**	**1.1 (0.5)**	**0.9**	**135**	**2.7**	**232**
3	17 Mar/leg 1	42.5/0.84/0.93/1.21	8.99/1.12/1.20/0.85	0.34/1.31/1.44/1.10	1.0 (0.3)	0.7	1482	3.4	231
4	17 Mar/leg 2	41.9/0.83/0.91/1.23	9.99/0.81/0.99/0.63	0.39/0.99/1.11/0.90	1.0 (0.3)	0.9	501	3.3	229
5	17 Mar/leg 3	37.5/0.83/0.99/1.15	9.80/0.83/1.31/0.64	0.43/0.97/1.32/0.88	1.0 (0.3)	0.4	682	3.4	226
6	*26 Mar*	*44.1/1.04/1.01/1.23*	*77.4/1.13/1.45/2.01*	*2.27/1.16/2.18/0.89*	*13.6 (21.1)*	*0.9*	*286*	*3.0*	*237*
7	**30 Mar/leg 1**	**34.9/0.79/1.07/1.18**	**8.70/0.83/5.71/0.53**	**0.39/1.18/4.65/1.50**	**1.2 (0.6)**	**0.7**	**308**	**3.3**	**221**
8	**30 Mar/leg 2**	**25.7/0.85/1.45/0.76**	**9.58/0.90/3.12/0.30**	**0.61/0.91/2.35/1.70**	**1.4 (0.9)**	**−0.8**	**498**	**4.0**	**214**
9	1 Apr	39.7/1.05/0.99/1.36	16.5/0.97/1.28/1.04	0.72/0.99/1.40/0.97	2.1 (1.8)	0.8	178	3.4	235
10	11 Apr/leg 1	34.7/0.95/1.10/1.52	19.2/1.59/1.60/1.01	0.81/1.67/1.57/0.92	2.4 (1.3)	−0.2	1108	1.5	225
11	11 Apr/leg 2	29.7/0.94/1.21/1.82	15.1/0.95/1.01/0.71	0.80/0.86/1.36/0.63	2.4 (1.3)	−0.2	160	1.5	215
12	17 Apr	41.6/0.99/1.08/1.45	57.1/1.24/1.38/1.77	1.92/1.11/1.26/0.85	14.5 (17.8)	0.8	363	2.8	226
13	**22 Apr**	**20.9/1.47/2.04/1.77**	**11.5/1.36/8.26/0.47**	**0.81/1.01/4.57/3.24**	**1.4 (0.8)**	**−0.3**	**81**	**2.5**	**226**
14	*24 Apr*	*34.4/1.46/1.49/1.68*	*88.6/1.46/1.21/1.23*	*3.01/1.14/1.17/0.67*	*42.3 (47.3)*	*0.8*	*143*	*0.9*	*236*
15	11 Jun/leg 1	41.3/1.44/1.34/1.98	40.7/1.25/1.36/0.89	1.66/1.01/1.24/0.69	2.2 (0.9)	−0.1	317	3.5	235
16	11 Jun/leg 2	41.7/1.47/1.37/1.98	43.3/1.23/1.38/1.03	1.64/1.01/1.23/0.70	2.2 (0.9)	0.1	273	3.4	236
17	*12 Jun*	*49.7/1.14/1.04/1.33*	*40.5/1.38/1.67/2.17*	*1.19/1.18/1.65/0.71*	*13.9 (6.0)*	*0.9*	*227*	*3.6*	*243*

CloudSat are reasonable. To identify such periods for comparison, we estimate Z_e by integrating the measured PSD averaged over a distance comparable to a *CloudSat* footprint weighted by the backscatter coefficients of nonspherical particles calculated using a DDA algorithm as reported by Hong (2007). With this information, we seek to establish criteria based on discrepancies between in situ–estimated and *CloudSat*-measured Z_e. When the discrepancy is larger than some threshold, the clouds sampled by the SPEC Lear and *CloudSat* will be considered significantly different because of either the cloud field heterogeneity or the cloud temporal changes or advection between the sample times. The deviation of in situ–estimated Z_e assuming different particle habits is generally less than ~5 dBZ_e (Deng et al. 2010; Okamoto 2002). So we expect that any threshold will be larger than this value.

In Table 2, we list the correlation coefficients of cloud properties between 2D-S products and satellite retrievals (2C-ICE/DARDAR/2B-CWC-RVOD or *CALIPSO* extinction) from data that are sampled with different thresholds of Z_e discrepancy. We see from Table 2 that as the Z_e discrepancy decreases from 20 to 8 dBZ_e, the correlation coefficients increase monotonically for all quantities. We also examine the Z_e discrepancies as a function of Δt, the minimum distance between the Lear and *CloudSat*, the standard deviations of in situ measurements, and a cloud field variability parameter derived

from MODIS reflectances that is contained in the level-2B cloud geometrical profile product (2B-GEOPROF) dataset. We find that the Z_e discrepancies are well correlated with the in situ–measured cloud variability when the discrepancies are less than 15 dBZ_e. We speculate that cloud spatial inhomogeneities and temporal variations are a likely explanation for the better agreement for the cases with lower Z_e discrepancy. While the scatter between in situ measurements and the cloud parameters derived from A-Train are reduced as we set tighter Z_e thresholds, we find that the qualitative conclusions of this study are not dependent on the threshold chosen. In other words, while the variances of the comparisons to in situ data are dependent on the discrepancy threshold, the overall biases between the in situ–derived quantities and the retrieved products are not a function of the threshold. Therefore, in the following discussion, we focus on the bias and the relative variation in scatter among the various products using comparisons where the Z_e discrepancy threshold is set at 10 dBZ_e, unless otherwise stated. Using the Z_e–IWC relation in Hogan et al. (2006) and error propagation analysis, we get

$$\partial \text{IWC}/\text{IWC} = \ln 10 \times 0.062 \times \partial Z_e. \quad (1)$$

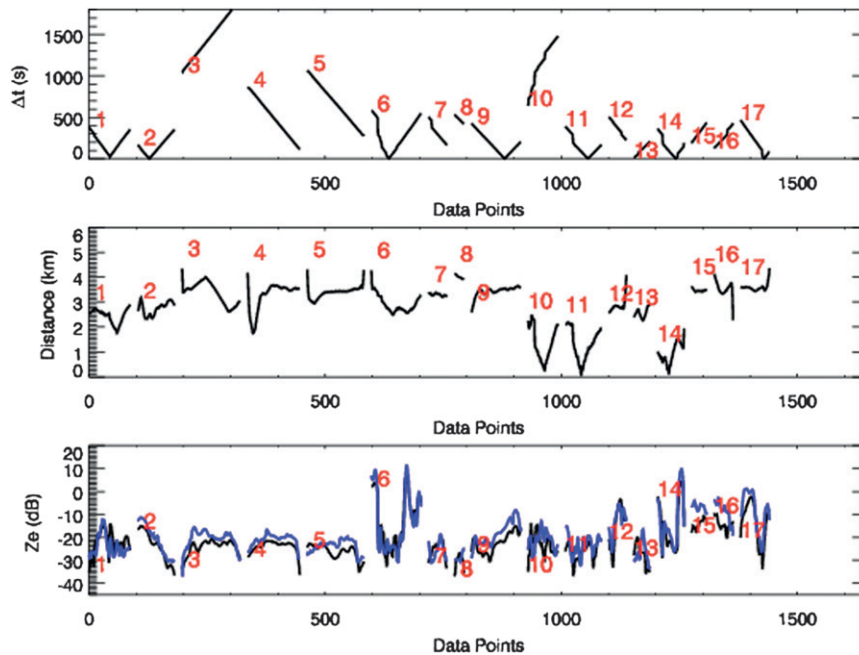So, for a 10-dBZ_e difference, the relative uncertainty of IWC is about 138%.

FIG. 2. (top) Time duration Δt between the SPEC Lear 25 and NASA A-Train satellite for 17 coordinated flight legs from January to June 2010. (middle) Minimum distance between the SPEC Lear 25 and NASA A-Train. (bottom) *CloudSat*-measured or 2C-ICE-parameterized radar reflectivity in the lidar-only region (blue) and simulated radar reflectivity (black) from 2D-S-measured particle size distribution, mass–size, and area–size relations on SPEC Lear 25.

4. Retrieval case studies

Because the nature of the retrieval methodology and subsequent results are very dependent on the vertical measurement region (lidar only, radar–lidar, and radar only) we present four cases in different cloud scenes to see how the retrieval results compare with each other and with in situ measurements.

a. Case 1: Radar–lidar overlap

On 1 April 2010, the SPEC Lear 25 was coincident with the A-train overpass and flew near the top of a cirrus layer with mean optical depth of about 2, which was observed by both the *CloudSat* radar and *CALIPSO* lidar (Fig. 3). The latitude and height plot of DARDAR extinction (Fig. 3c) has a similar envelope as *CALIPSO* (Fig. 3d) in the lidar measurement zone, because DARDAR uses the *CALIPSO* lidar feature mask to identify ice clouds. However, it has rough edges since it has to eliminate noise at 1.3-km horizontal resolution. For one data point at the flight level, we averaged the 2D-S measurements by 1 min and satellite retrieval datasets for 240 m in the vertical and 5 km in horizontal directions. The retrieved r_e (Fig. 3f) from 2C-ICE and DARDAR are in close agreement and closely follow the

situ measurements, while the 2B-CWC-RVOD is generally biased larger by about 35%. The retrieved IWC from 2C-ICE, DARDAR and 2B-CWC-RVOD at 38.4°– 38.8°N agree very well with the in situ measurements. But for 38.8°–39.0°N, the retrieved IWC is larger, while for 38°–38.4°N, the retrieval is biased smaller than the IWC derived from the in situ measurements. The extinction comparisons are similar.

Discrepancies between the retrieval results and the in situ data could be caused by the sampling location differences between the SPEC Lear and the A-Train

TABLE 2. The list of correlation coefficients r of cloud properties between 2D-S measurements and satellite retrievals (2C-ICE/ DARDAR/2B-CWC-RVOD or *CALIPSO* extinction) from datasets subsampled with different thresholds of Z_e between *Cloud-Sat*-measured and 2D-S-simulated for 17 flight legs. One set of comparisons from datasets selected using a discrepancy threshold less than 10 dBZ_e is shown in Fig. 7.

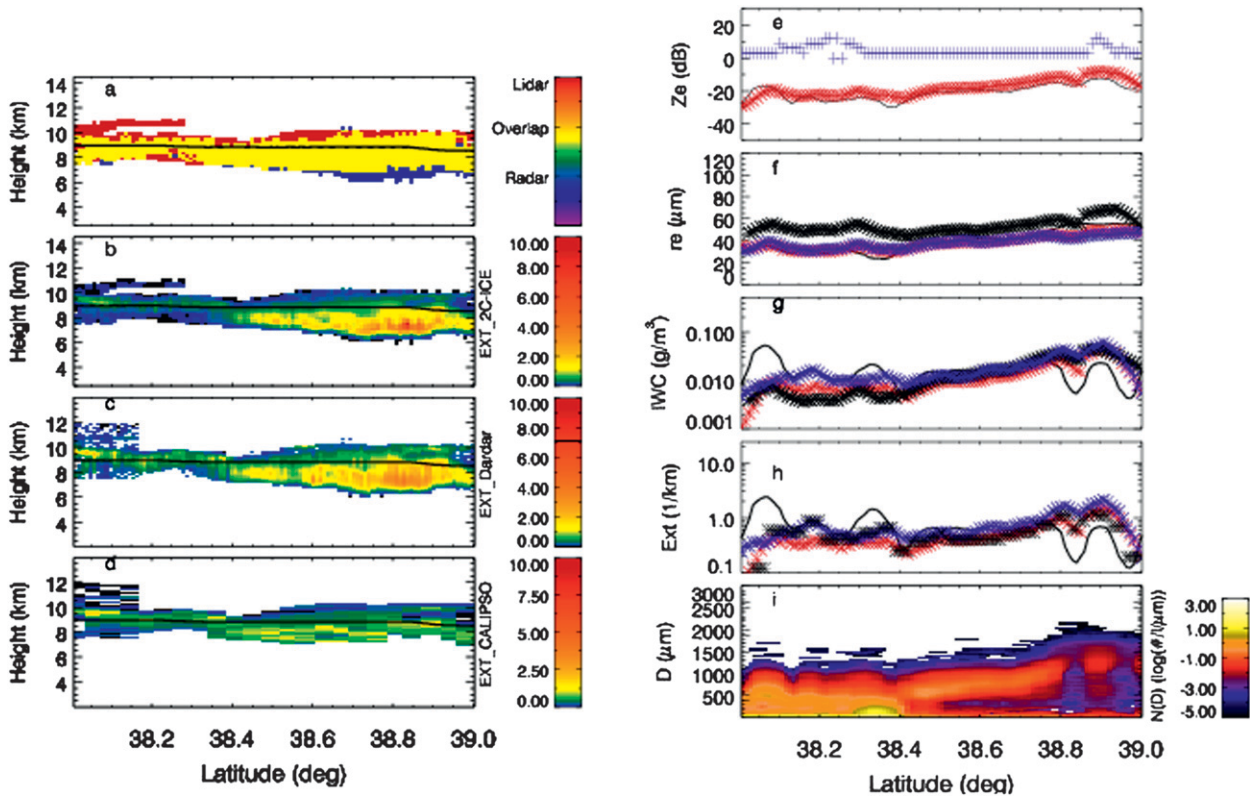| ΔZ_e threshold	r_r_e	$r\_$IWC	$r\_$extinction
<20	0.66/0.55/0.56	0.82/0.83/0.84	0.79/0.77/0.42
<15	0.69/0.59/0.59	0.88/0.87/0.90	0.85/0.81/0.43
<10	0.74/0.66/0.64	0.91/0.91/0.93	0.89/0.87/0.62
<8	0.76/0.67/0.66	0.94/0.92/0.95	0.92/0.82/0.66

FIG. 3. Height–latitude cross sections of (a) radar–lidar observation zones from 2C-ICE product for the 1 Apr 2010 case and extinctions from (b) 2C-ICE, (c) DARDAR, and (d) *CALIPSO* products. Also shown are (e) the measured radar reflectivity (blue) and derived radar reflectivity (black) from 2D-S measurements on the Lear 25 and comparisons of (f) r_e, (g) IWC, and (h) extinction from 2C-ICE (red asterisks), DARDAR (blue asterisks), 2B-CWC-RVOD (black asterisks), and 2D-S measurements (black line). (i) 2D-S-measured particle size distribution $N(D)$. The MODIS variability index from the *CloudSat* 2B-GEOPROF product is multiplied by 5 and over-plotted in (e) with blue plus signs. It ranges from 1 to 5, corresponding to the *CloudSat* scene indices highly uniform, uniform, weakly variable, variable, and high variable.

(3–4 km), and cloud variations between the sample times (6 min), as well as the sample errors associated with the instruments. The discrepancy between simulated and measured radar reflectivity from *CloudSat* sheds some insight on the discrepancy of our comparison. We see from Fig. 3e that the measured Z_e are larger than the simulated radar reflectivity from 38.8° to 39°N, while for 38°–38.2°N, the simulated radar reflectivity values are slightly larger than the CPR-measured Z_e. Moreover, the spatial variations of cloud properties in both regions are larger than the other regions as shown in Fig. 3b. In Fig. 3e, we overplot the MODIS variability index from the *CloudSat* 2B-GEOPROF product. The MODIS variability indices range from 1 for very uniform to 5 for very heterogeneous (Mace 2007). Hence larger horizontal heterogeneity are located at 38.8°–39°N and 38°–38.2°N. Therefore, the cirrus layer variability in these two regions likely contributes to the discrepancies between the retrieval results and the in situ measurements.

The cases observed on 11 April and 11 June are also thin clouds observed by both *CloudSat* and *CALIPSO*. However, the correlations between the simulated and measured Z_e (Table 1) are very poor, which causes significant differences between the in situ measurement and retrieval results as listed in Table 1, while the DAR-DAR and 2C-ICE results are very close to each other, which indicates that the SPEC and A-Train instruments sampled different portions of the cirrus layer.

b. Case 2: A radar–lidar overlapped and radar-only retrieval

On 17 April, the SPEC Lear 25 flew through a thick anvil layer with mean optical depth around 15. The layer exhibited significant horizontal gradients in cloud physical thickness and cloud microphysical properties (Fig. 4). Besides the lower portion observed by radar only, the *CALIPSO* feature mask also missed the semitransparent clouds at 36.7°N and some part of radar–lidar overlapped region, where the signal may be below
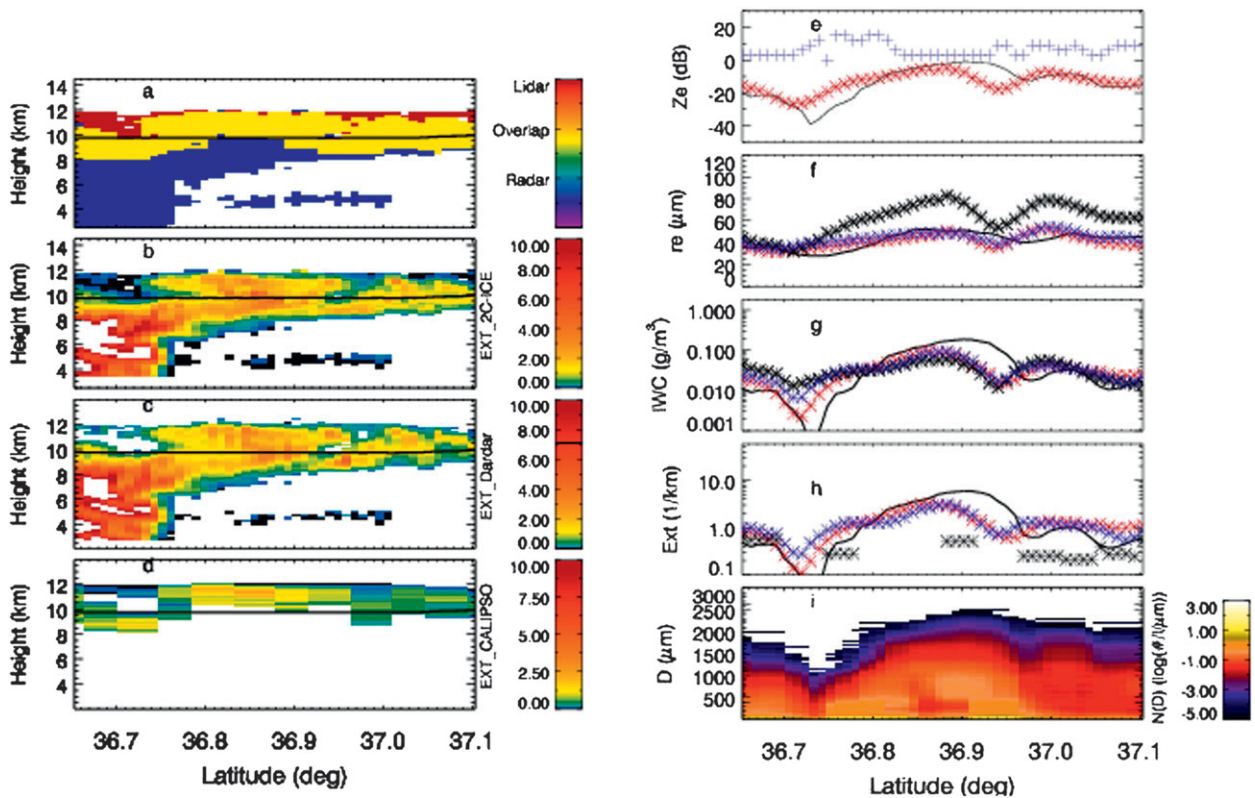
FIG. 4. As in Fig. 3, but for the thick-anvil case on 17 Apr 2010.

the *CALIPSO* cloud identification threshold at 5-km resolution (Liu et al. 2009). All in all, the magnitude of σ and morphology are very similar between 2C-ICE and DARDAR; however, 2C-ICE picks up more clouds with small σ around the cloud boundaries.

Similar to case 1, r_e from 2C-ICE and DARDAR agree well with in situ measurements, while 2B-CWC-RVOD is biased larger by ~45%. The IWC from 2C-ICE, DARDAR, and 2B-CWC-RVOD are very close. The dip at 36.95°N is not observed by in situ measurement. Retrieved extinctions from 2C-ICE and DARDAR are very close to the in situ measurements except the dip at 36.95°N. The larger disagreement between retrieval and in situ measurement at 36.74° and 36.95°N is again collocated with regions of significant heterogeneity as indicated by the MODIS variability index in Fig. 4e.

The *CALIPSO* extinction, whenever there is a value, is generally smaller than the other retrieval results and the in situ measurements. The discrepancy may be caused by the 5-km averaging of signals when the horizontal gradient in this complex scene is large, since the retrieval of σ is highly nonlinear with respect to β. This systematic bias of *CALIPSO* σ in thick clouds was also observed in Mioche et al. (2010) when compared with in

situ measurements during the Cirrus Cloud Experiment (CIRCLE-2).

c. Case 3: Lidar-only retrieval

On 22 April, the SPEC Lear 25 flew through a thin cirrus layer that had relatively large spatial variations and was mainly observed by the *CALIPSO* lidar (Fig. 5). The spatial variations are not well represented by the MODIS variability index because the cloud remained generally optically thin. The *CloudSat* CPR-observed short segments at 39.1° and 39.2°N at the 9-km level. Figure 5e shows the *CloudSat* CPR-measured Z_e and 2C-ICE-parameterized Z_e in the lidar-only region. We find that the parameterized radar reflectivity in the lidar-only region is less than approximately -30 dBZ_e. The correlation between the 2C-ICE Z_e and the in situ–simulated radar reflectivity is very poor. One must keep in mind, however, that the purpose of parameterizing the radar reflectivity in the lidar-only regions is to provide the retrieval algorithm with a constraint so that the numerical inversion can proceed seamlessly through the layer. Our approach simply tells the algorithm that the reflectivity in this region is smaller than the *CloudSat* radar minimum sensitivity
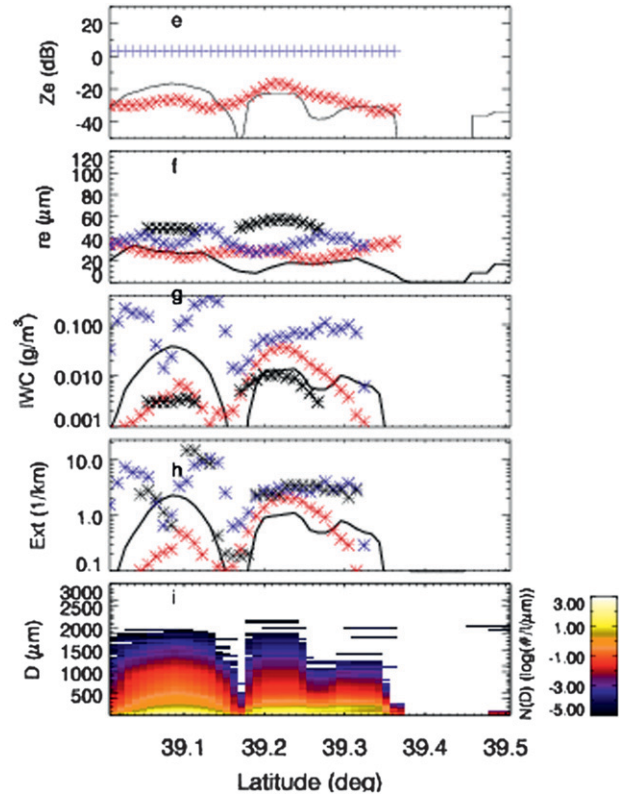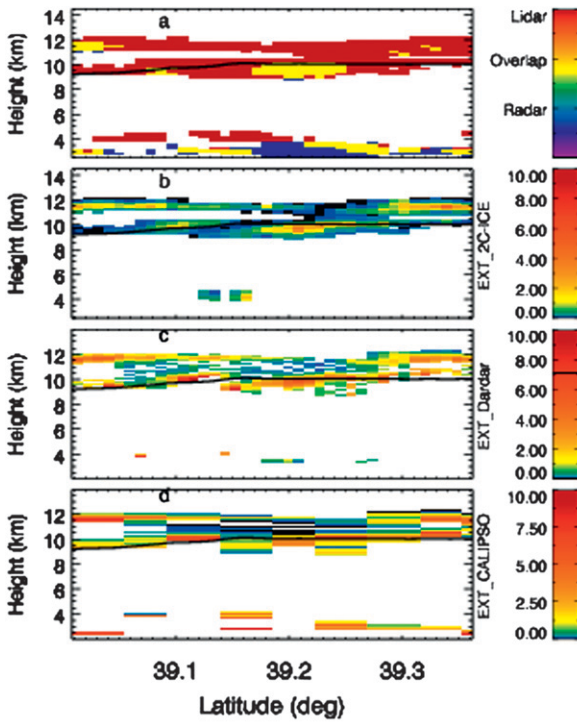
FIG. 5. As in Fig. 3, but for a thin-cirrus case on 22 Apr 2010.

but highly uncertain. For this purpose, the approach is useful.

For the radar–lidar overlap region at 39.2°N, the 2C-ICE retrieval and IWC from 2B-CWC-RVOD agree well with in situ measurements, but for radar–lidar overlap region at 39.1°N, the retrieved IWC and extinction from 2C-ICE are smaller than in situ measurement since the observed radar reflectivity by *CloudSat* CPR is smaller than that simulated from the in situ data.

The correlation between the 2C-ICE and DARDAR extinction is very poor. The DARDAR retrieval is close to 2C-ICE only for the short radar–lidar overlap periods at 39.1° and 39.2°N. For the lidar-only region, r_e, IWC, and σ from DARDAR are larger than 2C-ICE and also larger than itself in the sections where radar and lidar are overlapping. This appears to be an inconsistency in DARDAR because if it were correct, then the simulated radar reflectivity in the lidar-only region would be even larger than the radar–lidar region. These results suggest that the technique of parameterizing the radar reflectivity in the lidar-only region to provide a weak Z_e constraint allows 2C-ICE to provide more consistent results than the DARDAR product in lidar-only regions. The σ from *CALIPSO* is larger than 2C-ICE and in situ measurements. The final lidar ratio in the *CALIPSO* extinction

retrieval is found to be reduced by 50% from the initial value for the flight mean, This is the only flight among the 17 flights with significant reduction in *CALIPSO* lidar ratio.

The 30 March cases are very similar to the 22 April case discussed above: a thin cirrus case mainly observed by *CALIPSO* lidar. As shown in Table 1 for these three legs, DARDAR-retrieved IWC and σ, as well as the *CALIPSO* σ, are significantly overestimated.

d. Case 4: An opaque ice cloud

On 12 June, the SPEC Lear 25 flew through the middle of an optically thick ice cloud near the boundaries of our defined radar-only and radar–lidar overlapped region where *CALIPSO* is heavily attenuated (Fig. 6). Again, the 2C-ICE algorithm identified more clouds with smaller extinction coefficients around the cloud boundaries than did the DARDAR algorithm. The simulated and measured radar reflectivities in Fig. 6e have a high correlation coefficient (0.9) and small discrepancy. 2B-CWC-RVOD r_e is still biased larger than the other retrieval datasets and in situ measurements by ~30%. IWC and extinctions from the retrievals are close to the in situ measurements except around the 42.3°N, where the 2C-ICE is smaller than DARDAR but close to the in situ measurements.
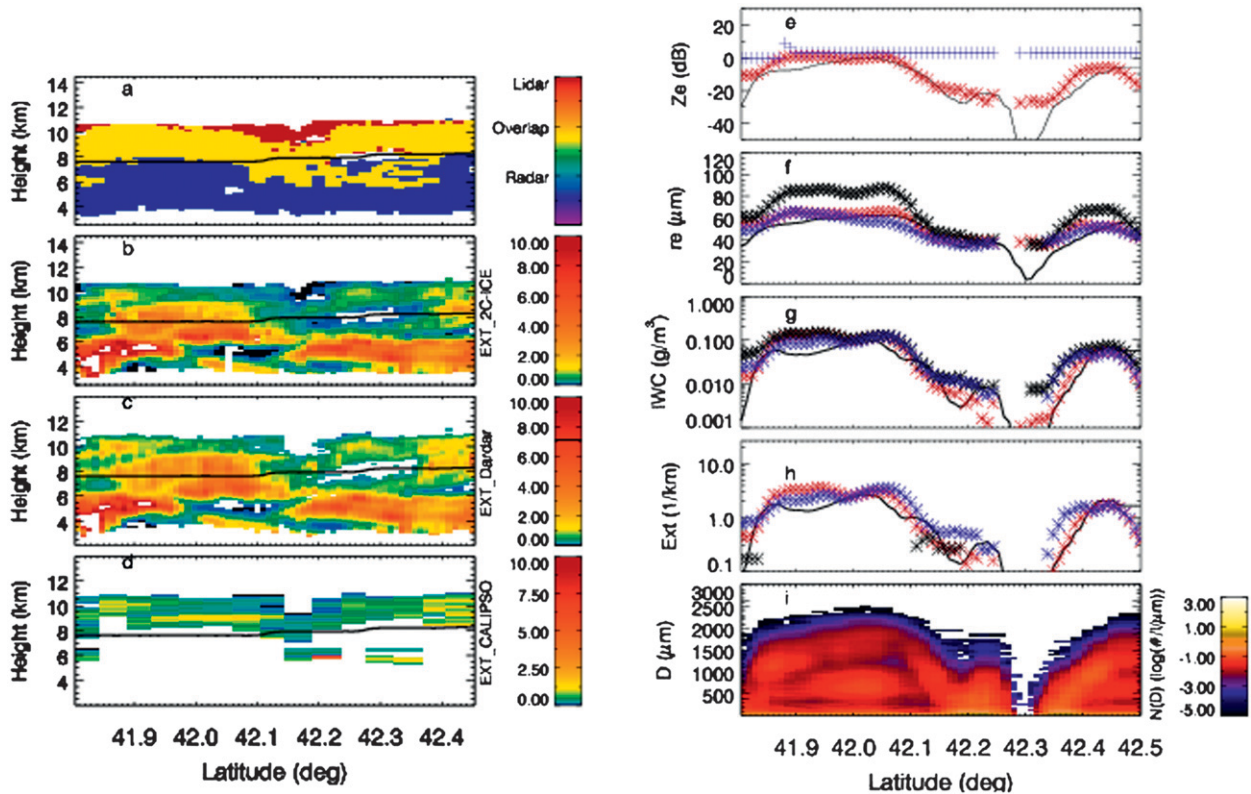
FIG. 6. As in Fig. 3, but for a thick-cirrus case on 12 Jun 2010.

5. Statistical comparison and discussion

Figures 7–9 show statistical comparisons of the retrieved IWC, r_e, and σ from the satellite algorithms compared to 2D-S cloud properties for the 17 underflights of the A-Train by the Lear 25 during SPARTICUS. Overall, we find that 2C-ICE and DARDAR show a generally strong agreement with one another and with the in situ measurements. This consistent performance can be seen in Fig. 7 where the three quantities (IWC, r_e, and σ) are strongly correlated with the in situ data with minimal overall bias although the scatter is around a factor of 2 for IWC and σ, which is about the scale of uncertainty derived from Eq. (1) for a 10-dBZ_e discrepancy between in situ–derived and *CloudSat*-measured radar reflectivities. The histograms (Fig. 8) confirm the generally strong agreement between the in situ data and 2C-ICE and DARDAR. However, subtle differences in the retrieved datasets that were identified in the case studies seem to emerge as well in the histograms and the

flight mean ratios. The IWC for instance shows a strong modal peak near 0.1 g m^{-3} that the retrievals and the in situ data both produce. 2C-ICE, however, seems to show a tendency to have a frequency of occurrence of low IWC that is more frequent than the 2D-S, and DARDAR seems to capture the overall distribution with more fidelity than 2D-S. Breaking the IWC distribution in regions where radar contributes to the retrieval and where lidar contributes to the retrieval, it seems as though the higher occurrence of low IWC seems to be more frequent in the lidar regions. This tendency can also be seen in the flight mean ratios in Fig. 9 with a persistent IWC ratio slightly less than 1 for 2C-ICE relative to the in situ data. DARDAR, in the flight mean statistics does appear to be more scattered overall than 2C-ICE. This variability can be identified in Fig. 7 and the slightly lower correlation coefficient for σ and IWC.

The visible extinction coefficient shows a strong bimodal structure with a primary mode near 0.5 km^{-1} and a secondary peak near 1 km^{-1}. It seems evident that 2C-ICE and DARDAR are able to capture the essential characteristics of these distributions. However, both algorithms tend not to produce the secondary mode near 1 km^{-1} as frequently as does the 2D-S. It can be seen that this tendency is more pronounced in the lidar region. The
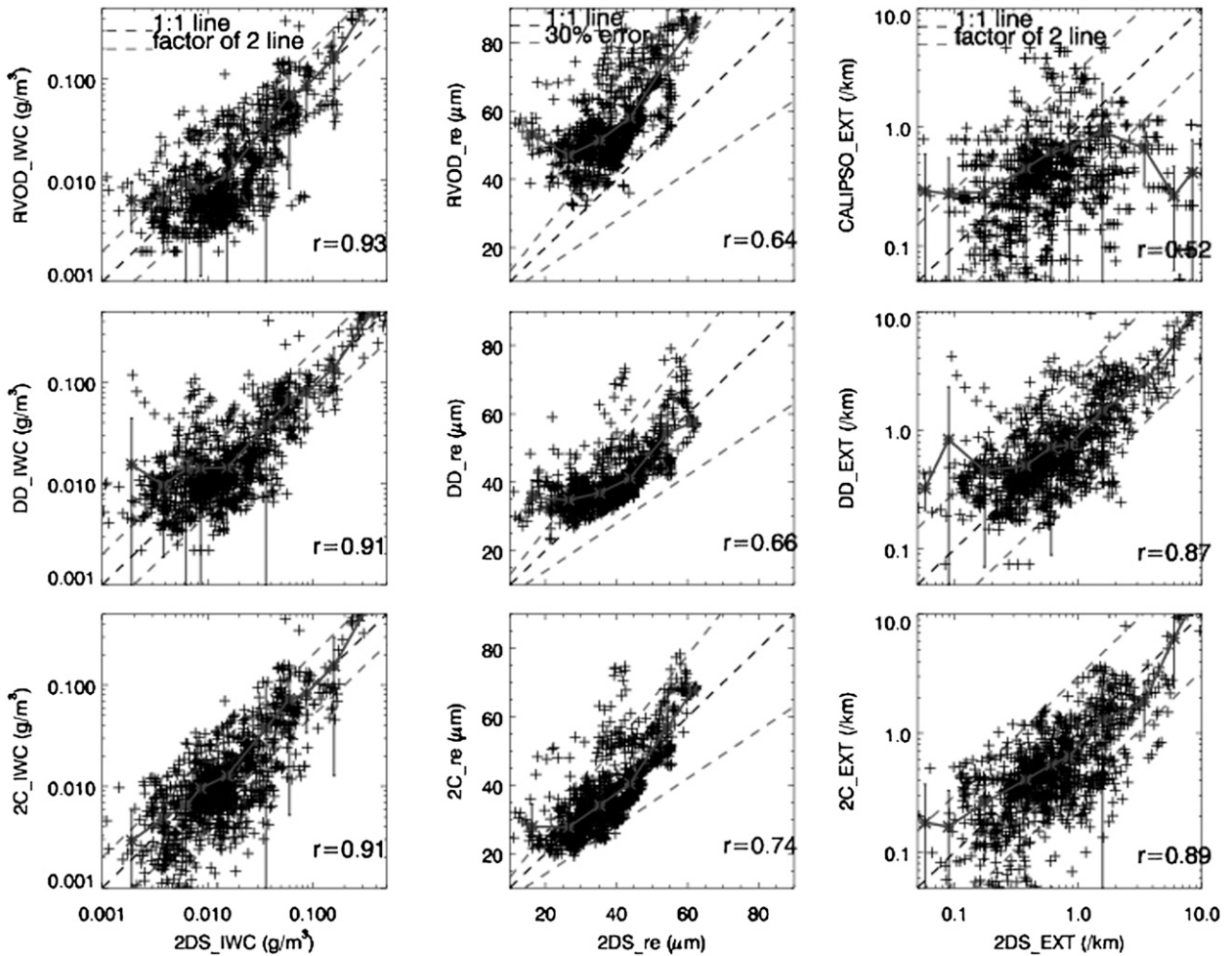
FIG. 7. The scatterplots of retrieved cloud properties in comparison with 1-min 2D-S measurements from the subsampled dataset when radar reflectivity discrepancy is less than 10 dBZ_e. (bottom) 2C-ICE, (middle) DARDAR, and (top) 2B-CWC-RVOD and *CALIPSO* extinction. The correlation coefficients r are noted in each panel. The grey solid lines are the mean.

CALIPSO σ histogram does not seem to reproduce the 1 km^{-1} peak very well although the agreement at the smaller values of extinction seems strong. This bias in the *CALIPSO* extinction can be identified in the scatterplots in Fig. 7 and in the flight means statistics in Fig. 9.

The r_e frequency distributions for all data combined have a single peak near 30 μm. Both 2C-ICE and DARDAR tend to make this peak too prominent in comparison with the in situ data. We further divide the data to the lidar region and radar region instead of lidar-only or radar-only region to increase the number of data points in each subset. For the radar region, DARDAR and 2C-ICE are very close to one another. For the lidar region, the probability density for small particles around 20 μm increases for in situ measurements and 2C-ICE, but not for DARDAR. This better correlation of 2C-ICE r_e with in situ–measured r_e than DARDAR r_e can be

identified in the scatterplots in Fig. 7 too. Therefore, we find that 2C-ICE seems to reproduce the r_e histogram with somewhat more fidelity than DARDAR.

The problems with 2B-CWC-RVOD that are discussed in the case studies are strikingly evident in the statistical comparisons where a slightly low bias in the IWC and a significant high bias in the r_e is evident even though the correlation coefficients of 2B-CWC-RVOD with 2D-S are similar to DARDAR and 2C-ICE.

Relationships among remote sensing measurables and cloud microphysical properties are shown in Fig. 10. The Z_e–IWC relations from in situ, 2C-ICE, and DARDAR datasets in Fig. 10a are generally consistent with one another. The IWC-normalized extinction and radar reflectivity are plotted as a function of effective radius in Figs. 10b and 10c for data filtered for the 10-dBZ discrepancy between in situ–derived and *CloudSat*-measured
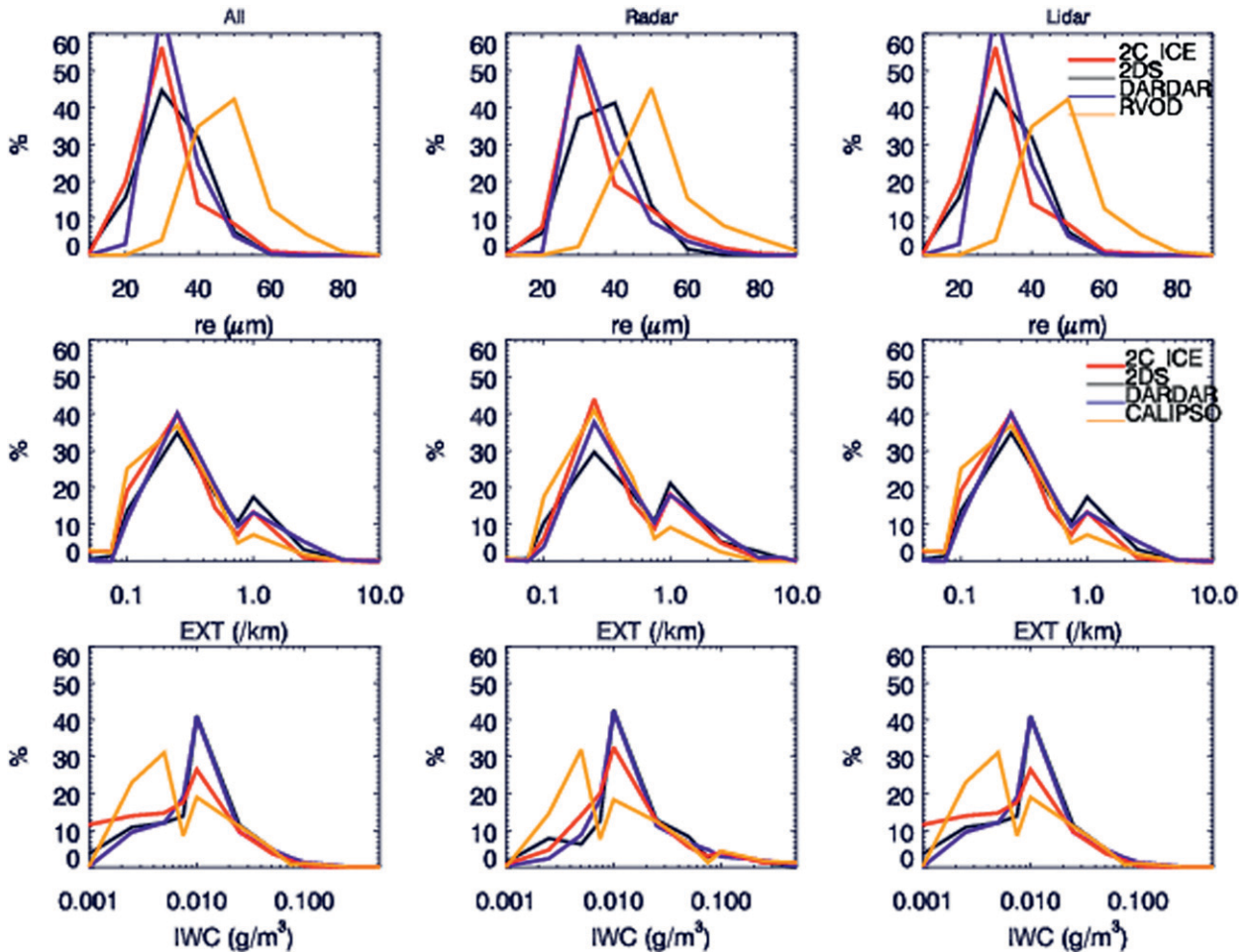
FIG. 8. Histogram comparisons of cloud properties such as r_e, extinction, and IWC between retrieval datasets and 2D-S measurements. The three columns are for all regions (including lidar only, radar–lidar, and radar only), lidar region, and radar regions, respectively. See the text for more details.

values. These two relations are very sensitive to the ice particle size–ice particle mass and ice particle size–ice particle cross-sectional area empirical relations assumed in the algorithms but more strongly a function of the ice bulk microphysics and radar and lidar measurements than the size–mass and size–area relations themselves. Therefore they are used here to illustrate the discrepancies among algorithm results and in situ measurements. The in situ data are, overall, very scattered. For extinction (Fig. 10b), 2C-ICE and DARDAR agree reasonably well with in situ measurements. For Z_e (Fig. 10c), the 2C-ICE results follow the 2D-S measurements but intersect with DARDR data at about 0 dBZ, while 2B-CWC-RVOD is shifted to the left by about 20 μm with respect to 2C-ICE. This may explain why the 2B-CWC-RVOD r_e is significantly larger than the other retrieval results and in situ measurements. Considering the similarity in the Z_e–IWC relationships and the disparity in Z_e–IWC-size relation

for 2B-CWC-RVOD when evaluated with the other products suggests that the size–area empirical relation in 2B-CWC-RVOD is very different from other algorithms since r_e is defined as the ratio of mass to area.

6. Summary

In this study we evaluate four published ice cloud retrieval algorithms that use some combinations of A-Train data against in situ measurements that were collected during the SPARTICUS field campaign. The datasets evaluated include *CloudSat* 2C-ICE and 2B-CWC-RVOD standard products, the DARDAR retrievals, and extinctions derived by the *CALIPSO* team. The case studies show that cloud spatial and temporal variations are considerable requiring the data to be carefully screened for consistency before reasonable comparisons can be made. Because SPARTICUS collected data under
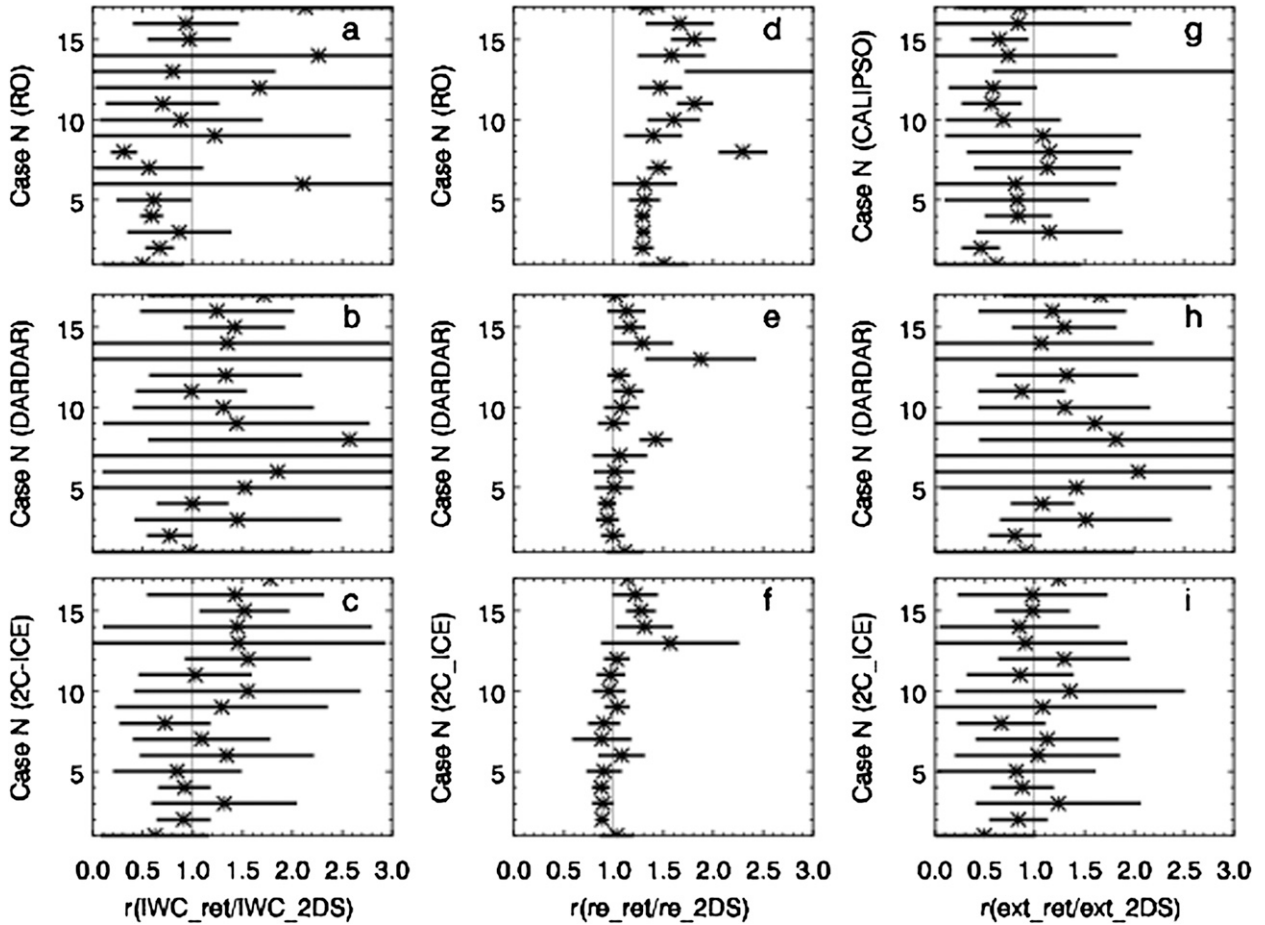
FIG. 9. Flight mean ratio and std dev of retrieved-to-measured IWC, r_e, and extinction for each retrieval method. These results are for the dataset selected using radar reflectivity discrepancy less than 10 dBZ_e. For 2B-CWC-RVOD (*CALIPSO* extinction), the average is for regions with radar (lidar) measurements.

21 overpasses of the A-Train in various types of cirrus over a period of six months, we are still able to make reasonable statistical evaluations of the datasets even after carefully removing inconsistent sections of flight legs. The discrepancies between the in situ–simulated and *CloudSat* radar-measured Z_e appears to be a reasonable indicator for spatial or temporal inhomogeneity to guide the comparisons. When the discrepancy between remotely sensed and in situ–derived Z_e is less than 10 dBZ_e, the flight mean ratios of retrieved-to-estimated IWC for 2C-ICE, DARDAR, and 2B-CWC-RVOD are 1.12, 1.59, and 1.02, respectively. For r_e, the flight mean ratios are 1.05, 1.18, and 1.61, respectively. For extinction, the flight mean ratios for 2C-ICE, DARDAR, and *CALIPSO* are 1.03, 1.42, and 0.97, respectively.

The *CloudSat* 2C-ICE product is in very close agreement generally with the DARDAR dataset. However,

using a parameterized radar reflectivity in the lidar-only regions of ice layers in the 2C-ICE algorithm does seem to provide an extra useful constraint since it effectively informs the algorithm that the radar reflectivity is less than the minimum measurable *CloudSat* radar reflectivity. The DARDAR algorithms tend to overestimate IWC and extinction in the lidar-only region in the cases examined here. The differences in mass–size and area–size relations between *CloudSat* 2C-ICE and DARDAR may also contribute to some subtle difference between the two datasets. It is also interesting to note that the more sophisticated approaches to treating multiple scattering of the lidar signal and the lidar ratio in DARDAR do not seem to provide significant benefit over the simple treatment in 2C-ICE as compared with the in situ data. It is likely that other sources of uncertainties, such as the mass–dimensional and area–dimensional assumptions as well as the assumption of the functional forms of the
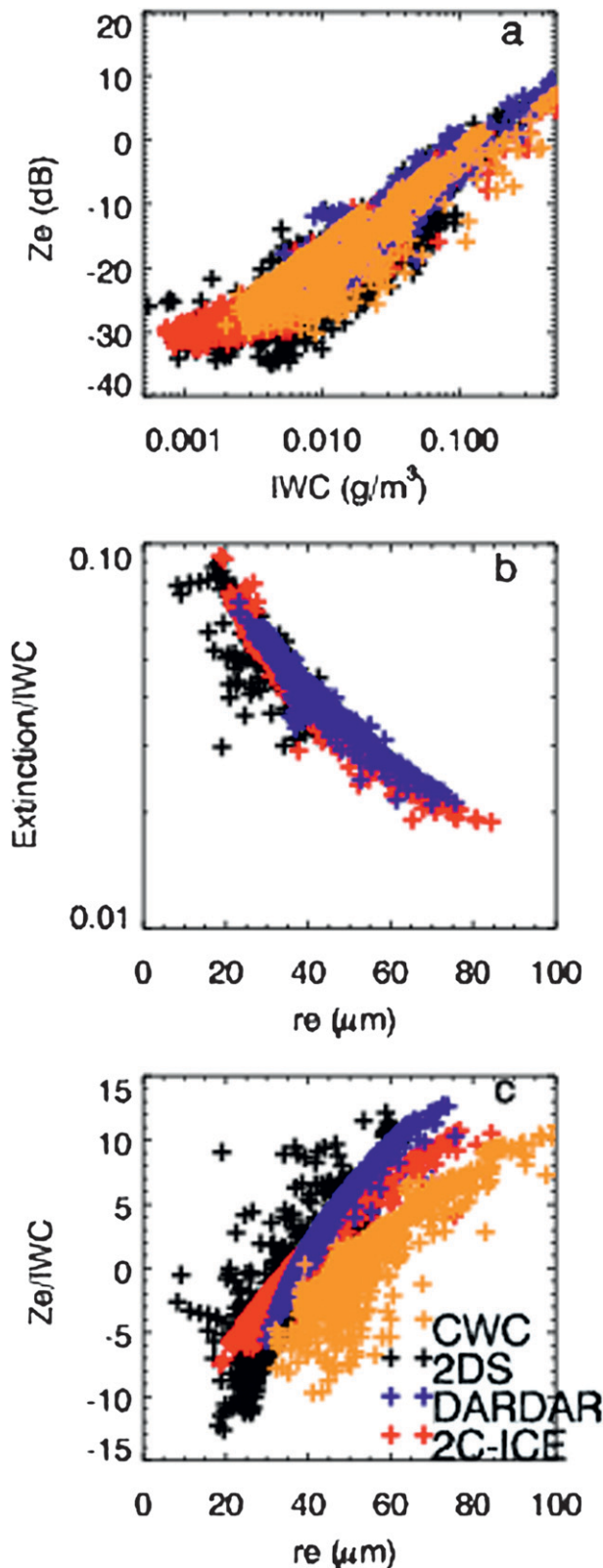
particle size distributions, are more significant sources than the treatment of lidar multiple scattering and lidar ratio. It is likely that these more sophisticated methodologies will be beneficial once these other sources of uncertainty can be reduced.

The r_e from the 2B-CWC-RVOD dataset is significantly biased larger than the other retrieval products and in situ measurements by about 40%. The assumption of solid spherical ice particles with bulk ice density might be responsible for this bias.

For *CALIPSO* extinction at 5-km resolution, the underestimation found from this study and Mioche et al. (2010) may be due to 5-km averaging when the clouds generally have spatial scales of variability that are smaller than this averaging length. The lidar ratio assumptions in the *CALIPSO* retrieval is probably one of the factors affecting the lidar extinction comparisons. Compared to *CALIPSO* and DARDAR, *CloudSat* 2C-ICE picks up more cloud volume around cloud boundaries with low extinction and IWC, either because of a lenient ice cloud identification threshold in the lidar-only region or because of a coarser vertical resolution.

Last, we note that while there are differences in the details, the use of radar–lidar synergy in cirrus cloud property retrieval does seem to provide a very reasonable approximation of what is actually observed in nature. This is a significant finding because it suggests that A-Train retrieval results can be used to investigate the important processes that maintain cirrus in the global atmosphere and that parameterizations of these processes can be confidently developed from these data for eventual implementation in global models.

FIG. 10. Comparisons of (a) Z_e–IWC relations and (b) IWC-normalized extinction or (c) radar reflectivity as a function of r_e from 2C-ICE (red crosses), DARDAR (blue crosses), 2B-CWC-RVOD (orange crosses), and 2D-S measurement (black crosses).

REFERENCES

Abernethy, R. B., and R. P. Benedict, 1984: Measurement uncertainty: A standard methodology. *ISA Trans.,* **24,** 75–79.

Ackerman, T. P., and G. M. Stokes, 2003: The Atmospheric Radiation Measurement Program. *Phys. Today,* **56** (1), 38–44.

Austin, R., and G. L. Stephens, 2001: Retrieval of stratus cloud microphysical parameters using millimeter-wave radar and visible optical depth in preparation for *CloudSat*: 1. Algorithm formulation. *J. Geophys. Res.,* **106,** 28 233–28 242.

——, A. J. Heymsfield, and G. L. Stephens, 2009: Retrieval of ice cloud microphysical parameters using the *CloudSat* millimeter-wave radar and temperature. *J. Geophys. Res.,* **114,** D00A23, doi:10.1029/2008JD010049.

Baker, B. A., and R. P. Lawson, 2006: Improvement in determination of ice water content from two-dimensional particle imagery. Part I: Image to mass relationships. *J. Appl. Meteor. Climatol.,* **45,** 1282–1290.

Bevington, P. R., and D. K. Robinson, 1992: *Data Reduction and Data Analysis for the Physical Sciences*. McGraw-Hill, 328 pp.

Brown, P. R. A., and P. N. Francis, 1995: Improved measurements of the ice water content in cirrus using a total-water probe. *J. Atmos. Oceanic Technol.,* **12,** 410–414.

Delanoë, J., and R. J. Hogan, 2008: A variational scheme for retrieving ice cloud properties from combined radar, lidar, and infrared radiometer. *J. Geophys. Res.,* **113,** D07204, doi:10.1029/2007JD009000.

——, and ——, 2010: Combined *CloudSat–CALIPSO*–MODIS retrievals of the properties of ice clouds. *J. Geophys. Res.,* **115,** D00H29, doi:10.1029/2009JD012346.

Deng, M., G. G. Mace, Z. Wang, and H. Okamoto, 2010: Tropical Composition, Cloud and Climate Coupling Experiment validation for cirrus cloud profiling retrieval using *CloudSat* radar and *CALIPSO* lidar. *J. Geophys. Res.,* **115,** D00J15, doi:10.1029/2009JD013104.

Field, P. R., R. J. Hogan, P. R. A. Brown, A. J. Illingworth, T. W. Choularton, and R. J. Cotton, 2005: Parameterization of ice particle size distributions for mid-latitude stratiform cloud. *Quart. J. Roy. Meteor. Soc.,* **131,** 1997–2017.

Francis, P. N., P. Hignett, and A. Macke, 1998: The retrieval of cirrus cloud properties from aircraft multi-spectral reflectance measurements during EUCREX'93. *Quart. J. Roy. Meteor. Soc.,* **124,** 1273–1291.

Froberg, C.-E., 1965: *Introduction to Numerical Analysis*. Addison–Wesley, 340 pp.

Heymsfield, A. J., and Coauthors, 2008: Testing IWC retrieval methods using radar and ancillary measurements with in situ data. *J. Appl. Meteor. Climatol.,* **47,** 135–163.

Hogan, R. J., 2006: Fast approximate calculation of multiply scattered lidar returns. *Appl. Opt.,* **45,** 5984–5992.

——, M. P. Mittermaier, and A. J. Illingworth, 2006: The retrieval of ice water content from radar reflectivity factor and temperature and its use in the evaluation of a mesoscale model. *J. Appl. Meteor. Climatol.,* **45,** 301–317.

Hong, G., 2007: Radar backscattering properties of nonspherical ice crystals at 94 GHz. *J. Geophys. Res.,* **112,** D22203, doi:10.1029/2007JD008839.

Im, E., C. Wu, and S. L. Durden, 2006: Cloud profiling radar for the *CloudSat* Mission. *IEEE Trans. Aerosp. Electon. Syst.,* **20,** 483–486.

Korolev, A. V., 2007: Reconstruction of the sizes of spherical particles from their shadow images. Part I: Theoretical considerations. *J. Atmos. Oceanic Technol.,* **24,** 376–389.

——, and G. A. Isaac, 2005: Shattering during sampling by OAPs and HVPS. Part I: Snow particles. *J. Atmos. Oceanic Technol.,* **22,** 528–542.

——, J. W. Strapp, and G. A. Isaac, 1998: Evaluation of the accuracy of PMS optical array probes. *J. Atmos. Oceanic Technol.,* **15,** 708–720.

——, E. F. Emery, J. W. Strapp, S. G. Cober, G. A. Isaac, M. Wasey, and D. Marcotte, 2011: Small ice particles in tropospheric clouds: Fact or artifact? Airborne Icing Instrumentation Evaluation Experiment. *Bull. Amer. Meteor. Soc.,* **92,** 967–973.

Lawson, R. P., 2011: Effects of ice particles shattering on the 2D-S probe. *Atmos. Meas. Tech.,* **4,** 1361–1381.

——, D. O'Connor, P. Zmarzly, K. Weaver, B. Baker, and Q. Mo, 2006: The 2D-S (stereo) probe: Design and preliminary tests of a new airborne, high-speed, high-resolution particle imaging probe. *J. Atmos. Oceanic Technol.,* **23,** 1462–1477.

——, E. Jensen, D. L. Mitchell, B. Baker, Q. Mo, and B. Pilson, 2010: Microphysical and radiative properties of tropical clouds investigated in TC4 and NAMMA. *J. Geophys. Res.,* **115,** D00J08, doi:10.1029/2009JD013017.

Liu, C. L., and A. J. Illingworth, 2000: Toward more accurate retrievals of ice water content from radar measurement of clouds. *J. Appl. Meteor.,* **39,** 1130–1146.

Liu, Z., and Coauthors, 2009: The *CALIPSO* lidar cloud and aerosol discrimination: Version 2 algorithm and initial assessment of performance. *J. Atmos. Oceanic Technol.,* **26,** 1198–1213.

Mace, G. G., 2007: Level 2 GEOPROF product process description and interface control document algorithm version 5.3. Jet Propulsion Laboratory, 44 pp.

——, 2010: Cloud properties and radiative forcing over the maritime storm tracks of the Southern Ocean and North Atlantic derived from A-Train. *J. Geophys. Res.,* **115,** D10201, doi:10.1029/2009JD012517.

——, Q. Zhang, M. Vaughan, R. Marchand, G. Stephens, C. Trepte, and D. Winker, 2009: A description of hydrometeor layer occurrence statistics derived from the first year of merged *Cloudsat* and *CALIPSO* data. *J. Geophys. Res.,* **114,** D00A26, doi:10.1029/2007JD009755.

Mace, J., E. Jensen, G. McFarquhar, J. Comstock, T. Ackerman, D. Mitchell, X. Liu, and T. Garrett, 2009: SPARTICUS: Small Particles in Cirrus science and operations plan. U.S. Department of Energy Tech. Rep. DOE/SC-RM-10-003, 15 pp. [Available online at http://www.arm.gov/publications/program docs/doe-sc-arm-10-003.pdf.]

Mioche, G., D. Josset, J. F. Gayet, J. Pelon, A. Garnier, A. Minikin, and A. Schwarzenboeck, 2010: Validation of the *CALIPSO*–CALIOP extinction coefficients from in situ observations in midlatitude cirrus clouds during the CIRCLE-2 experiment. *J. Geophys. Res.,* **115,** D00H25, doi:10.1029/2009JD012376.

Mitchell, D. L., R. P. D'Entremont, and R. P. Lawson, 2010: Inferring cirrus size distributions through satellite remote sensing and microphysical databases. *J. Atmos. Sci.,* **67,** 1106–1125.

Okamoto, H., 2002: Information content of the 95-GHz cloud radar signals: Theoretical assessment of effects of nonsphericity and error evaluation of the discrete dipole approximation. *J. Geophys. Res.,* **107,** 4628, doi:10.1029/2001JD001386.

Sassen, K., Z. Wang, and D. Liu, 2009: Cirrus clouds and deep convection in the tropics: Insights from *CALIPSO* and *CloudSat*. *J. Geophys. Res.,* **114,** D00H06, doi:10.1029/2009JD011916.

Stephens, G. L., and Coauthors, 2008: *CloudSat* mission: Performance and early science after the first year of operation. *J. Geophys. Res.,* **113,** D00A18, doi:10.1029/2008JD009982.

——, and Coauthors, 2010: Dreary state of precipitation in global models. *J. Geophys. Res.,* **115,** D24211, doi:10.1029/2010JD014532.

Toon, O. B., and Coauthors, 2010: Planning, implementation, and first results of the Tropical Composition, Cloud and Climate Coupling Experiment (TC4). *J. Geophys. Res.,* **115,** D00J04, doi:10.1029/2009JD013073.

Twohy, C. H., A. J. Schanot, and W. A. Cooper, 1997: Measurement of condensed water content in liquid and ice clouds using an airborne counterflow virtual impactor. *J. Atmos. Oceanic Technol.,* **14,** 197–202.

Winker, D. M., M. A. Vaughan, A. H. Omar, Y. Hu, K. A. Powell, Z. Liu, W. H. Hunt, and S. A. Young, 2009: Overview of the *CALIPSO* mission and CALIOP data processing algorithms. *J. Atmos. Oceanic Technol.,* **26,** 2310–2323.

Yang, P., K. Liou, K. Wyser, and D. Mitchell, 2000: Parameterization of the scattering and absorption 25 properties of individual ice crystals. *J. Geophys. Res.,* **105,** 4699–4718.

Young, S. A., and M. A. Vaughan, 2009: The retrieval of profiles of particulate extinction from *Cloud-Aerosol Lidar Infrared Pathfinder Satellite Observations* (*CALIPSO*) data: Algorithm description. *J. Atmos. Oceanic Technol.,* **26,** 1105–1119.